Bulletin of the Seismological Society of America, Vol. 99, No. 2B, pp. 968–979, May 2009, doi: 10.1785/0120080068

Review: Rotations in Structural Response

by M. D. Trifunac

Abstract Measurements of point rotations in full-scale structures during earthquake excitation do not exist at present, but average rotations can be computed from pairs of parallel transducers. The examples presented illustrate rotations in the range from 10^{-6} to 10^{-3} rad and angular accelerations from 10^{-4} to 10^{-1} rad/sec^2. Measurements of rotations in the structures for excitation by microtremors are also described. It is argued that recording the rotational components of motion contributes significantly to the overall volume and quality of information. It is recommended that the development and deployment of instruments to measure rotational components of motion in free-field conditions and in full-scale structures will open a new frontier for advanced experimental identification of structural properties and for structural health monitoring.

Introduction

Studies of the rotational components of ground motion preceded and have lasted longer than either the modern seismology (late 1800s to present) or the engineering strong-motion seismology (1930s to present) (Trifunac, 2009a). In the 1700s, it was believed that earthquakes were caused by explosions in the earth, and so instruments were designed to detect tilting rather than horizontal and vertical motions. A bowl filled with mercury was used by de la Haute Feuille in 1703 to determine the direction of the shock (Favaro,1884; Baratta, 1895; Davison, 1927). After the earthquakes at Lisbon, 1755, and Calabria, 1783, interest in rotational waves increased. Robert Mallet (1810–1881) studied the rocking of surface objects and analyzed the forces governing their motion (Ferrari 2006; Kozák, 2006). Rotational motions were also studied by Charles Lyell (1797–1875), Charles Darwin (1809–1882), and Alexander von Humboldt (1769–1859). In 1875, Filippo Cecchi designed an electrical seismograph to record rotations on sliding smoked paper, but it was not sensitive enough to obtain any traces of rotational motions. However, Checchi's instrument was the first true seismograph (Cecchi, 1876; Agamennone, 1906). It had three pendulums to record north–south (N–S), east–west (E–W), and vertical motions, a device to measure rotations, and magnification of about three times. It recorded the first true seismographs during a large earthquake on the French–Italian border in 1887 (Denza, 1887).

The significance of the contribution of ground rotation to recorded seismographs was debated at length during late nineteenth century (Milne, 1893; Schlüter, 1903; Wiechert, 1903), before introduction of seismographs capable of recording vertical ground motion. Later experiments with measured vertical ground motion showed that the role of ground tilting in linear-wave motion is usually small. Galitzin (1902), who doubted the conclusions based on those experiments, formulated the theory of the transducer response, subjected simultaneously to tilts and displacements. However, he found it so complicated that in his later work he was forced to neglect the effects of tilts (Galitzin, 1904). The interest among seismologists in the rotational components of motion diminished after Gutenberg (1927) wrote that such waves cannot propagate, and that if they are generated at the source they will be attenuated quickly. It took another half century before more complete descriptions of the relative role of three translations and three rotations, acting simultaneously on the simple transducer, were published (Graizer, 1980; Trifunac and Todorovska, 2001a).

In earthquake engineering, the recognition that the rotational components of strong motion contribute significantly to the response started to appear much later, around the 1960s (Trifunac 2006). So far, the main use of rotations in engineering design has been in the area of interstory drifts and in correlations of the maximum drifts with damage levels (Trifunac and Ivanović, 2003; Ghobarah, 2004; Trifunac, 2009b). With increased interest in performance-based design and structural health monitoring, studies of the rotational components in excitation and in response are now beginning to appear. The measurement of point rotations may evolve into a useful tool for identification of nonlinear deformations and for temporal and spatial identification of plastic hinges in structures (Gičev and Trifunac, 2008).

Rotational components of ground motion and their effects on obelisks, grave stones, and buildings are mentioned in many older texts, which by describing the consequences of strong shaking also aimed to decipher its physical nature (Davison, 1927; Imamura, 1937; Richter, 1958). The combined effects on man-made structures of differential ground motions, ground strains, and curvatures, and of torsional (Luco, 1976; Lee and Trifunac, 1985) and rocking ground

accelerations (Lee and Trifunac, 1987) can be considerable. Differential excitation of flexible, extended, multiple, and separate foundations (as in bridges; see Werner *et al.* [1979]) can lead to large pseudostatic shears and moments in structural members (Trifunac and Todorovska, 1997a; Trifunac and Gičev, 2006; Jalali and Trifunac, 2008). The large torsional responses of tall buildings in Los Angeles during the San Fernando earthquake in 1971 were ascribed to torsional ground motion (Hart *et al.*, 1975), while longitudinal differential ground motions may have caused the collapse of bridges during the 1971 San Fernando, 1978 Miyagi-ken-Oki (Bycroft 1980), and 1994 Northridge (Trifunac *et al.*, 1996) earthquakes. Earthquake damage to pipelines that is not associated with faulting or landslides but rather with large differential motions, strains, and curvatures in the soil, reflects the consequences of traveling seismic waves and of the associated large rotations and twisting of soil blocks caused by lateral spreads and by early stages of liquefaction (Ariman and Muleski, 1981; Trifunac and Todorovska, 1997b, 1998).

The aim of this article is to describe briefly the sources and the amplitudes of rotational motions that are relevant for engineering analyses of the response of structures, and then to illustrate how rotations can be used to extend this information and to refine the resolution of the data on the full-scale response of structures. However, the material presented is neither comprehensive nor complete, and a description of many studies related to the rotational components of strong motion in structures will not be included. Laboratory experiments on the rotations of beam–column connections, and the associated computer simulations, for example, will not be discussed. This subject involves a voluminous body of literature and should be reviewed in detail, which is beyond our present scope.

Sources of Rotational Motion

For a macroscopic view of strong-motion rotations, we can start with kinematic representation of faulting (Bouchon and Aki, 1982; Graizer, 1989) and follow the radiated elastic waves and first-order linear theory of elasticity. More advanced considerations could involve the mechanics of incremental deformations (Biot, 1965), the microphysics of fracture in rocks (Teisseyre, 2002), and irreversible deformations from dislocations, disclinations, and microcracks (Teisseyre and Majewski, 2002; Teisseyre *et al.*, 2003). In the following review, only the linear macroscopic formulation will be considered.

Earthquake Source

Strong motion near faults is complicated by the irregular distribution of fault slip and by complex nonlinear processes, and it cannot be predicted in detail. A qualitative approach to characterizing these motions is to use displacements and displacement pulses that have been calibrated against the observed fault slip and the recorded strong motions in terms of their amplitudes in time and their spectral content, in what is essentially a dimensional analysis (Trifunac, 1993). Trifunac (2009b) shows examples, for a strike-slip fault, of two simple displacements in order to describe the growth of the fault-parallel displacement, d_N, toward the permanent static offset, and a pulse, d_F, that may be perpendicular to the fault. Relevant properties of such d_F and d_N functions for this work are their initial velocities $\dot{d}_{F,\max}$ and $\dot{d}_{N,\max}$ (Figs. 1 and 2) and the associated sudden and large rotations at the time of wave arrival, $\sim\dot{d}_{F,\max}/c_g$ and $\sim\dot{d}_{N,\max}/c_g$, where c_g is the horizontal phase velocity in the ground, $\beta < c_g < \alpha$, and α is the representative velocity of dilatational waves. It can be shown that $\dot{d}_{F,\max} \sim \sigma\beta/\mu_s$, where σ is the effective stress ($\sim$ stress drop) on the fault surface, β is the velocity of shear waves in the fault zone, and μ_s is the rigidity of rocks surrounding the fault. Also, $\dot{d}_{N,\max} = 0.5C_0\sigma\beta/\mu_s$ at $t = 0$, with $C_0 = 0.6$, 0.65, 1.00, 1.52, and 1.52 for M 4, 5, 6, 7, and 8, respectively (Trifunac, 1998). Because there are no strong-motion measurements of peak ground velocity, $v_{\max}$, at the fault surface, to measure $\dot{d}_{F,\max}$ and $\dot{d}_{N,\max}$, those can be estimated only indirectly, in terms of the estimates of stress drop, σ, on the fault plane, for example. In Figure 1, $\sigma \sim 2\mu_s\dot{d}_{N,\max}/(\beta C_0)$ (dotted lines) and $\sigma \sim \mu_s\dot{d}_{F,\max}/\beta$ (continuous lines) are shown for typical values of μ_s and β.

Figure 1 combines four scales along the x axis. The first scale, in bars (top axis, left), is used to plot examples of the stress-drop estimates from strong-motion data (e.g., Trifunac 1972a,b; Fletcher *et al.*, 1984). The numerical values of stress drop, measured in bars (1 bar = 10^6 dyne/cm^2) and of peak ground velocity $v_{\max}$ (top axis, right), measured

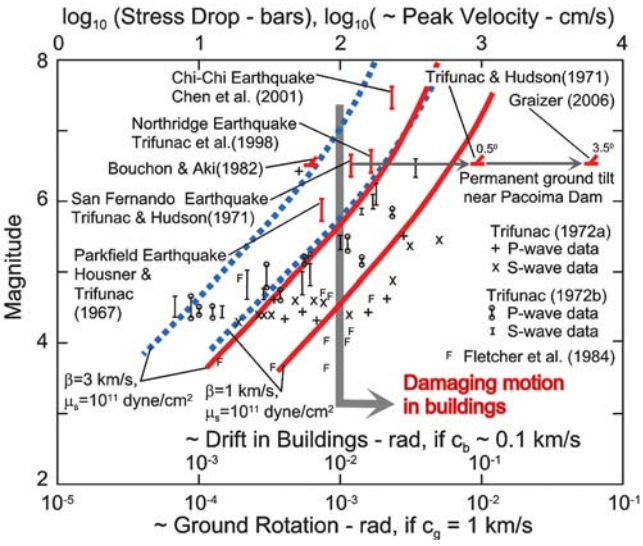

Figure 1. Stress drop estimates from near-field recordings (various symbols) and computed from $\dot{d}_F$ (solid lines) and $\dot{d}_N$ (dotted lines). Also shown are the corresponding order-of-magnitude estimates of peak ground rotations at the fault (assuming $c_g \sim 1$ km/sec) and of the drift in buildings (assuming $c_b \sim 0.1$ km/sec) (from Trifunac, 2009b).

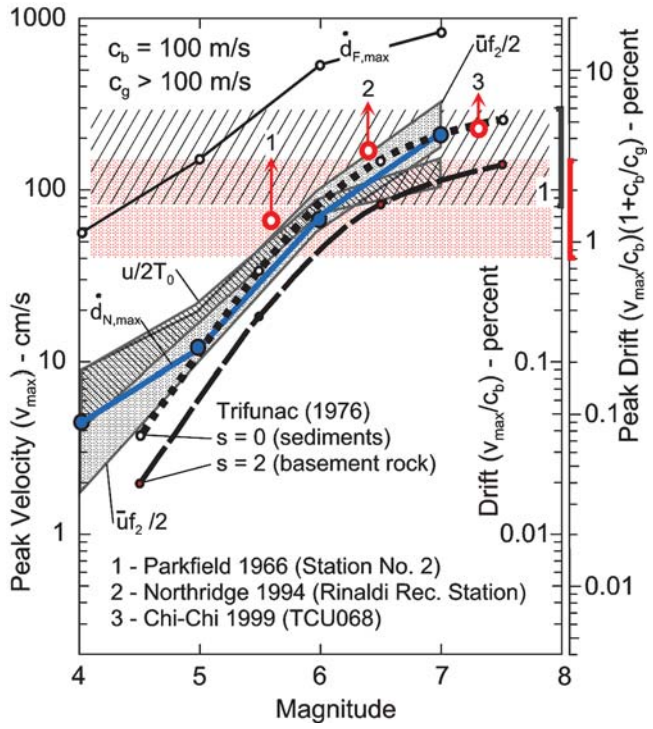

Figure 2. Comparison of peak ground velocities at or near faults, based on (1) $\dot{d}_{F,\max}$ and $\dot{d}_{N,\max}$; (2) lower bounds of the velocities of fault slip during rise time of dislocations ($\bar{u}/(2T_0)$ and $\bar{u}f_2/2$); and (3) empirical scaling equations for peak recorded velocities, extrapolated to the fault surface, at sites on sediments ($s = 0$) and on basement rock ($s = 2$). The right scale shows the range of peak drifts in simple buildings for $c_b \ll c_g$ (left), when ground rocking is neglected, and for $c_b \sim c_g$ (right), when ground rocking contribution to drift is included. Examples of peak velocities recorded close to the fault surface are shown for the Parkfield, Northridge, and Chi-Chi earthquakes (from Trifunac, 2009b).

in cm/sec coincide, because when $\beta = 3$ km/sec and $\mu = 3 \times 10^{11}$ dyne/cm^2, $v_{\max} \sim \sigma\beta/\mu$ gives

$$10^6 \text{ dyne/cm}^2 \times 3 \text{ km/sec} \times (1/3)10^{-11} \text{ cm}^2/\text{dyne} \times 10^5 \text{ cm/km} = \text{cm/sec}\,.$$

The peak rotation of strong motion, $\theta_{\max}$, can be approximated by $\theta_{\max} \sim v_{\max}/c_g$. Assuming that $c_g \sim 1$ km/sec, we construct in Figure 1 the third scale for peak ground rotations in rad/sec (bottom axis). Finally, assuming that a one-dimensional shear wave with peak velocity $v_{\max}$ propagates into a building, and that the vertical phase velocity in the building $c_b \sim 0.1$ km/sec (Todorovska and Trifunac, 2008), we can add the fourth scale to Figure 1 (bottom axis, inside), which gives the peak rotation ($\sim$ drift) in the building, drift $\sim v_{\max}/c_b$, in rad/sec. It can be seen that for the buildings located at or very close to surface faults, large peak velocities of ground motion will begin to damage the buildings for earthquakes with intermediate and large magnitudes.

As the distance between the fault and the recording site increases, attenuation will diminish the large initial strong-motion velocities at the fault $\dot{d}_{F,\max}$ and $\dot{d}_{N,\max}$. Figure 1 shows four such examples of recorded peak velocities during the 1966 Parkfield, 1971 San Fernando, 1994 Northridge, and 1999 Chi-Chi earthquakes. These were recorded close to the moving faults but could have been as much as 20 km away from the asperities producing the peak velocities. Figure 1 also shows the permanent rotations of ground (tilts) observed at the strong-motion accelerograph site on gneissic granite–diorite spine, about 20 m south of the southern abutment of the Pacoima Dam after the San Fernando (0.5°, Trifunac and Hudson, 1971) and Northridge (3.5°, Graizer, 2006) earthquakes. These rotations illustrate how much larger the permanent tilts can be following nonlinear site response (Trifunac, 2009b).

Peak Ground Velocity near Faults. For elongated faults, the duration of faulting can be approximated by $\tau_0 \sim L/v + 0.5W/\beta$, where L and W are fault length and width, v is the velocity with which the dislocation is spreading along the fault length, and β is the velocity of shear waves in the source region. One corner frequency, in the near-field spectra of strong-motion accelerations is then defined by $f_1 = 1/\tau_0$. The other corner frequency is $f_2 \sim 2.2/W$, and $1/f_2$ approximates the time for the dislocation to spread over the fault width W. Corner frequencies f_1 and f_2 can be estimated via extrapolation of empirical scaling of strong motion for $f <$ 0.1 Hz and by use of data on the fault length L, width W, dislocation amplitudes $\bar{u}$, and the stress drop (Trifunac, 1993; Trifunac and Novikova, 1995). Two low-bound estimates of the average dislocation velocity during its rise time, equal to $T_0 \sim \bar{u}\mu_s/(\sigma\beta)$ or $\sim 1/f_2$, are then $\bar{u}/(2T_0)$ or $\bar{u}f_2/2$. Peak ground velocity will be larger during the early phases of the fault motion and will subside for $t \gg T_0$. Figure 2 compares these lower-bound slip velocities, $\bar{u}/(2T_0)$ and $\bar{u}f_2/2$, with average peak ground velocity at zero epicentral distance, computed from corrected and integrated accelerograms (Trifunac, 1976). The line with short dashes shows average peak velocities at sites on sediments ($s = 0$), and the line with long dashes shows the same, but for the sites on the basement rock ($s = 2$). Figure 2 also shows three measured peak velocities relatively close to moving faults (for the 1966 Parkfield, 1994 Northridge, and 1999 Chi-Chi earthquakes). For these three examples, the recording stations were at some distance from the moving dislocations, and therefore the peak velocities on the fault surface would be expected to have been larger. This is implied in Figure 2 by arrows at points 1, 2, and 3.

Buildings near Faults. Depending upon the structural system (Ghobarah, 2004), collapse may occur for drifts larger than 0.8 to 3.0%—that is, for peak ground velocities larger than 80 to 300 cm/sec when $c_b \ll c_g$ (neglecting the effects of soil–structure interaction and of ground rocking) and 40 to 150 cm/sec when $c_b \sim c_g$ (again neglecting the effects of soil–structure interaction, but considering pseudostatic contributions to drift from ground rocking). This range of drifts

is emphasized in the two right-hand scales in Figure 2, and it is highlighted by two shaded zones within the figure. One of these scales describes the drift amplitudes in terms of $v_{\max}/c_b$, which is based on the traditional representation of the action of strong motion on structures in terms of horizontal motion only. The other (right-hand) scale shows the drift in the buildings amplified by the factor $(1 + c_b/c_g)$, when $c_b \sim c_g$, which approximates the contribution to the drift from the ground rocking (Trifunac, 2009b). It shows that the effects of strong-motion rotation are to amplify the relative structural response and the associated drifts by a factor, which depends on c_b/c_g. This illustrates that the largest pseudostatic effects of rotational ground motion will occur when the representative phase velocity of ground motion becomes small and comparable to the velocity of shear waves in the building. Perusal of the observed damage will also show that the observed trends are in agreement with the classical damage criteria of Duval and Fogelson (1962).

Wave Propagation Path

The waves radiated from the fault are changed along the propagation path through interference, focusing, scattering, and diffraction. For example, reflection of plane body waves from a half-space can lead to large displacement amplitudes, but the associated rotations change monotonically and do not lead to large amplifications (Trifunac, 1982; Lin *et al.*, 2005). Scattering and diffraction of waves from topographic features will lead to focusing and to amplification for both displacements and rotations (Sánchez-Sesma *et al.*, 2002). On ground surface near faults, the nonlinear response of soil, ground failure, and liquefaction will further contribute to large additional transient and permanent rotations.

Asymmetry of Support

Most man-made structures are constructed above the ground and can be tens of meters to several hundred meters high. Supported asymmetrically at the base, with the center of gravity near midheight, they undergo rocking motions when excited by earthquakes, winds, and man-made excitations. The soil–structure interaction then acts as a mechanism for conversion of the incident energy into rotational motions of the foundation, which radiates this wave energy back into the soil (Trifunac, 2008). Rotational motion of the ground accompanying the response of large buildings can be a significant factor for excitation of nearby small structures.

Artificial Strong Motion

In the absence of recorded rotational components of strong ground motion, it has been necessary for engineering studies to have at least preliminary but physically realistic simulations of such motions. The method of Lee and Trifunac (1985, 1987) meets some of these requirements in that it generates torsional and rocking accelerograms using an exact analytical method, assuming that (1) the motion occurs within a linear-elastic, layered half-space, and (2) synthetic ground motion can be constructed by superposition of body *P* and *SV* and surface Rayleigh waves for rocking and by body *SH* and surface Love waves for torsion.

Full-Scale Experiments

Full-scale experiments involving soil–structure interaction have provided data to interpret the nature of the motions of the soil caused by the building vibrations. The focus of most full-scale tests has been on the response of structures and on how it is affected by soil–structure interaction, but some experiments have investigated the nature of the near-field deformation of soil surrounding the building foundation (Luco *et al.*, 1975; Wong *et al.*, 1977). In densely populated metropolitan areas, where the separation distances between adjacent buildings are small, and where there are long bridges with multiple supports, detailed 2D and 3D analyses are required (Wong and Trifunac, 1975; Werner *et al.*, 1979). Studies of 2D soil–structure interaction have shown how the interference of the incident and scattered waves from the foundations can lead to nearly standing waves, which, at the nodes, results in strong torsional ground motions (Trifunac, 1972c). Studies of the response of 3D models show amplification of the torsional response of building–foundation–soil systems and the radiation of scattered torsional waves for near-horizontal incidence of *SH* waves (Lee, 1979). Studies of the wave-passage effects around rigid, embedded foundations have explained amplification of the rocking foundation motions and the more energetic radiation of rotational waves when half-wavelengths of the incident waves in the ground are comparable to the foundation width (Todorovska, 2002; Trifunac, 2008).

Rotations in Structural Response

Many earthquake response analyses model the n-degree-of-freedom systems by lumped masses interconnected with springs and dashpots, or by finite elements, but the accuracy of final representation ultimately depends upon the number of mode shapes included in the analysis and upon realistic representation of the boundary conditions. Because the computation of point rotations requires spatial differentiation of mode shapes, the computation of transient point rotations will require a large number (several hundred) of mode shapes to be included in the analyses. Because this is not practical, typical engineering calculations will represent a low-pass filtered approximation of point rotations.

Observations of Structural Response

When soil–structure interaction is considered in dynamic analyses, the assumption that the foundation is rigid simplifies the analysis and reduces the number of degrees of freedom required to model the system. Whether such an assumption can be made must be verified, and the outcome does not depend only on the relative rigidity of the founda-

tion and of the soil but also on the overall rigidity and type of the structure (Trifunac and Todorovska, 2001b; Todorovska, 2002). This can be illustrated by comparison of the N–S and E–W vibrations of the Millikan Library in Pasadena, California, a nine-story, reinforced-concrete structure. Even though the foundation system of this building is relatively flexible, for N–S vibrations two symmetric shear walls at the east and west ends of the building act to stiffen the foundation slab (Fig. 3a and c), and this allows one to proceed with a rigid foundation representation. For E–W vibrations, the building carries lateral loads by an elevator core, which deforms the foundation slab in the middle, while the shear walls act only as membranes providing axial constraints (Fig. 3b and d). Thus, for E–W vibrations the foundation slab cannot be approximated by a rigid foundation model. The 3D shapes of the warped foundation, which showed how this structure deforms while vibrating in N–S and E–W directions, were measured during forced-vibration tests (Foutch *et al.*, 1975). Figure 4 shows the relative contribution of horizontal deformation of soil (4%), roof displacement resulting from rigid body rocking (25%), and relative deformation of the building (71%) during steady-state forced vibrations in the N–S direction (as in Fig. 3a).

In the following, different aspects of rotational motions in two buildings—the Hollywood Storage Building (HSB), and the Van Nuys Hotel–Holiday Inn (VN7SH), both in the greater Los Angeles metropolitan area—are illustrated.

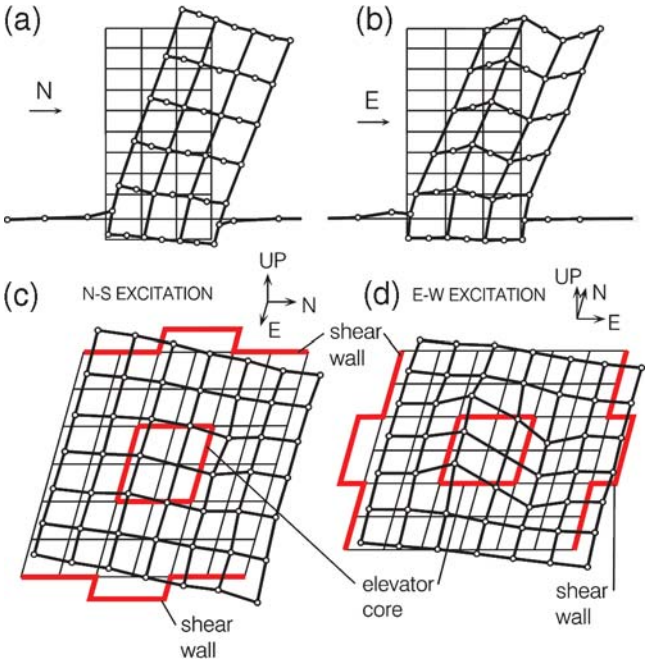

Figure 3. Deformation of the Millikan Library, a nine-story reinforced-concrete building, excited at the roof by a shaker (a) along the west shear wall during N–S excitation, (b) along a section through the elevator core during E–W excitation, (c) deformation of the basement slab during N–S excitation, and (d) deformation of the basement slab during E–W excitation (from Foutch *et al.*, 1975).

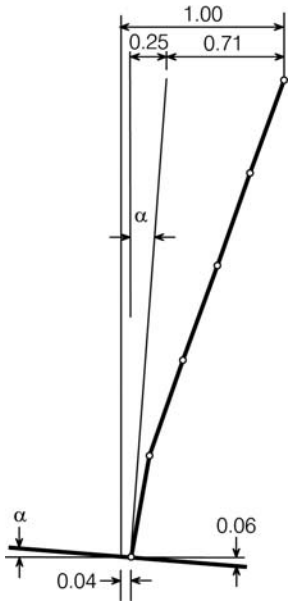

Figure 4. Contributions of foundation translation and rocking to the response of the Millikan Library for N–S shaking.

Hollywood Storage Building. This building (HSB in Fig. 5) was the first structure equipped with permanent strong-motion accelerographs in California, in 1933. It is also the first building in which strong motion was recorded (October 1933), and the first building for which it could be shown that theoretical analysis and observation of soil–structure interaction are mutually consistent (Duke *et al.*, 1970). Since 1933 there have been numerous triggers of strong-motion accelerographs in the HSB, but thus far only a few have been processed and are available for analysis (Trifunac *et al.*, 2001). HSB was also studied using ambient- and forced-vibration tests (Carder, 1936). The contributions of rocking and torsional components of strong ground motion to interaction were rarely addressed in the articles that aimed to interpret earthquake motions in buildings. Duke *et al.*

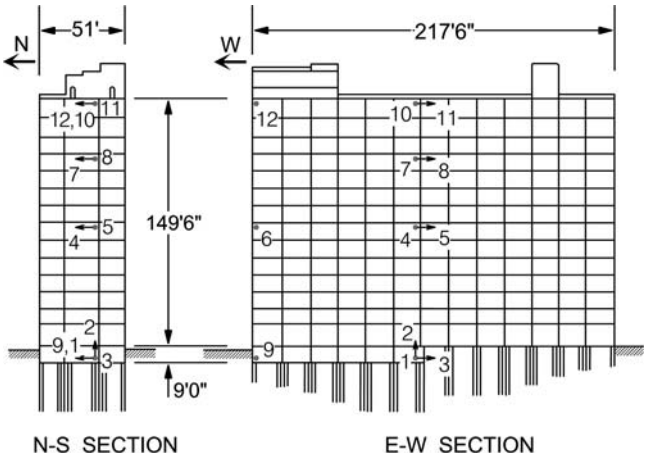

Figure 5. Location and orientations of 12 accelerometers maintained in the HSB by the California Division of Mines and Geology since 1976.

(1970) concluded that "soil–structure interaction produced marked change in the horizontal base displacements, in the E–W direction," with little or no rocking in this direction. For the N–S direction, soil–structure interaction did not drastically affect the horizontal base displacements but instead produced rocking of the foundation, which could be observed in terms of its effect on the roof motion (Trifunac *et al.*, 2001).

Torsion. Torsion in nonsymmetric structures is caused by geometrical separation of the centers of mass and of rigidity. For symmetric structures, torsion occurs because of a nonsymmetric foundation system or is excited by wave-passage effects (Luco, 1976; Trifunac, Ivanović, Todorovska, *et al.*, 1999), or both. Long and narrow symmetric buildings, for example, can experience significant torsion and whipping (Todorovska, 2002), especially when excited by ground waves propagating along the longitudinal axis of the soil–structure system.

Full-scale measurements of torsion cannot be performed directly because no rotational strong-motion accelerographs had been installed in the buildings in California during past strong earthquakes. It is only possible to estimate average rotations when recorders in the structures are arranged so that relative motions can be computed from the differences in translations. We illustrate this for HSB (Fig. 5). For example, $\phi_b(t) = [y_9(t) - y_1(t)]/3060$ (3060 cm is the separation distance between recorders 1 and 9) gives the average torsion at the foundation level, and $\phi_r(t) = [y_{12}(t) - y_{10}(t)]/3060$ gives average torsion of the western half of the building at the roof. Relative N–S vibrations at the center of the building are described by $y_{10}(t) - y_1(t)$, while $y_{12}(t) - y_1(t)$ gives the N–S motion at the roof, at the western end of the building, relative to the central station at the ground level. Then, $y_{12}(t) - y_{10}(t) - y_9(t) + y_1(t)$ gives the contribution to the motion of the western end of the building, at roof level, associated with the torsion of the building, relative to its base. Figure 6 illustrates these functions versus time for the motions recorded during the Landers earthquake of 1992. It can be seen that $y_{12}(t) - y_{10}(t) - y_9(t) + y_1(t) \sim y_{12}(t) - y_1(t)$ and that $y_{12}(t) - y_1(t) \sim 0.5[y_{10}(t) - y_1(t)]$. The relative motions at recording site 12 (western end of the building, on the roof) are about one-half the motions at recording site 10 (center of the building, on the roof), and the two motions are in phase. Thus, the building is twisting about a vertical axis that is west of its geometric center. Similar behavior was observed for a seven-story, reinforced-concrete building, also supported by a pile foundation (Trifunac, Ivanović, Todorovska, *et al.*, 1999). Such behavior may be caused in part by nonsymmetry of the foundation (the HSB has the basement only beneath its western half, Fig. 5). Thus, torsional eccentricity can cause whipping of the eastern end of the HSB, particularly for E–W arrivals of *SH* and Love waves.

Van Nuys Hotel–Holiday Inn. This building (VN7SH, Figs. 7 and 8) was damaged by the 1971 San Fernando and 1994 Northridge earthquakes (Ivanović *et al.*, 1999; Trifunac, Ivanović, and Todorovska, 1999). The reinforced-concrete structure, built in 1966, is 19.1 × 45.7 m in plan, has 7 stories, and is 20 m high. The structural damage in 1994 was extensive in the exterior south frame A (Fig. 7) but less severe in the north frame D; these frames were designed to take most of the lateral load in the longitudinal (E–W) direction. Severe shear cracks occurred at the middle columns of frame A, near the contact with the spandrel beam of the fifth floor, which decreased the capacity of the columns. Analysis of the relationship between the observed damage and the changes in equivalent vertical shear-wave velocity in this building can be found in Todorovska and Trifunac (2008). The 1994 response of VN7SH was recorded by a 13-channel CR-1 central recording system (channels 1 through 13 in Fig. 7) and by one triaxial SMA-1 accelerograph (channels 14, 15, and 16 in Fig. 7), with an independent recording system and a common trigger time.

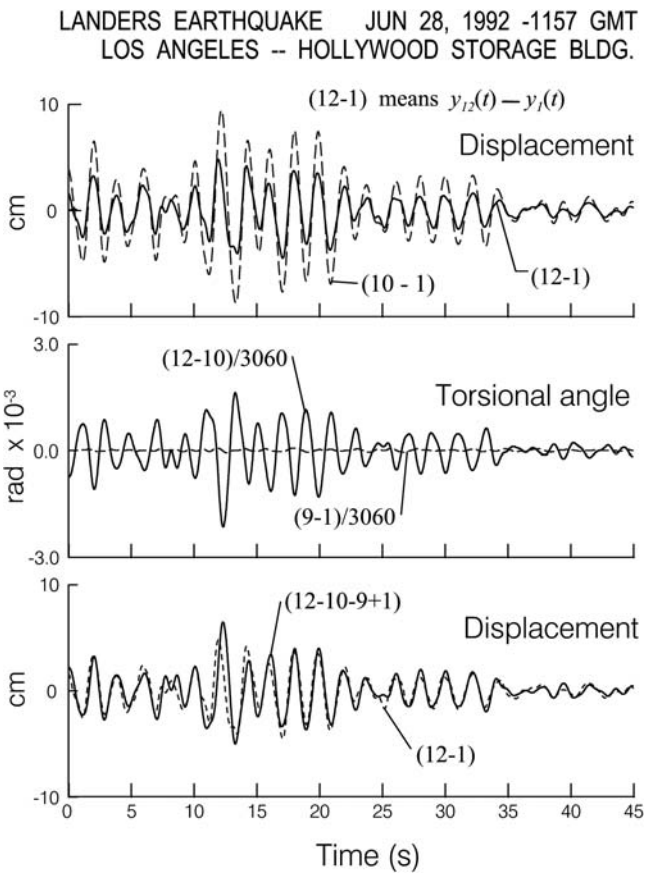

Figure 6. Response of the HSB during the Landers earthquake. (Top panel) Comparison of relative (with respect to basement-center) displacements recorded at the west end of the roof (12-1, solid line) and at the roof center (10-1, dashed line). (Center panel) Comparison of average torsion of the western half of the building ((12-10)/3060, solid line) and at ground level ((9-1)/3060, dashed line). (Bottom panel) Comparison of relative (with respect to basement-center) displacements at the west end of the roof due to torsion alone (12-10-9+1, solid line) and due to torsion and translation (12-1," dashed line).

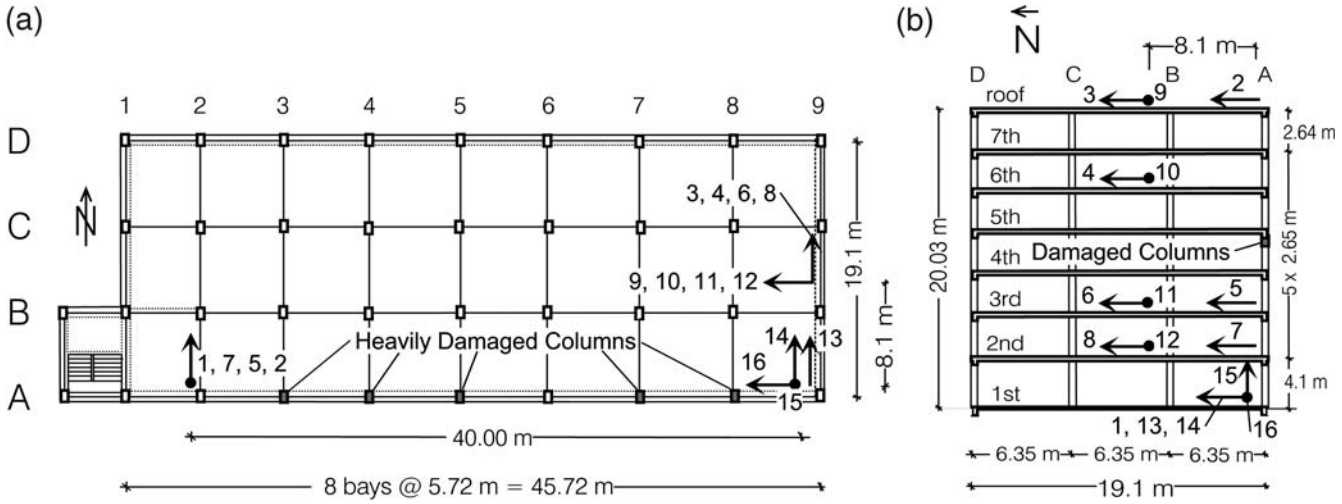

Figure 7. VN7SH building: (a) typical floor plan and (b) typical transverse section. Location and sensitivity axes of 16 acceleration transducers that have operated in this building since the mid-1970s.

Ambient-vibration tests in VN7SH have shown that the foundation supported by piles deformed during passage of microtremor waves and, therefore, also during passage of much larger strong-motion waves. The ambient-vibration tests also showed that the center of torsion for VN7SH is outside the building plan, close to its southeastern corner (Ivanović *et al.*, 1999). Analyses of strong-motion records have confirmed that this eccentricity may have been present in all post-1971 excitations, possibly associated with some asymmetry in the soil–pile system dating back to the construction of the building in 1966 or caused by damage to the piles during the 1971 San Fernando earthquake (Trifunac, Ivanović, Todorovska, *et al.*, 1999).

Rocking. Figure 9 compares the E–W rocking angles ([displacement at roof − displacement at ground level]/building height) versus instantaneous apparent frequency computed for most half-period segments of the response of the HSB during seven earthquakes. It can be seen that the apparent system frequency depends upon the amplitude of excitation and that for small amplitudes it approaches the frequency measured by Carder (1936) during full-scale ambient- and forced-vibration tests. These trends can be explained in terms of the conceptual soil–structure model shown in Figure 10. Nonlinear effects in the response of soil–structure systems depend upon the level of the excitation and also on the initial state of the system. The building damage changes the building permanently, but the soil can heal itself and recover the original stiffness by settlement with time and dynamic compaction from shaking during subsequent events (Todorovska, 2009).

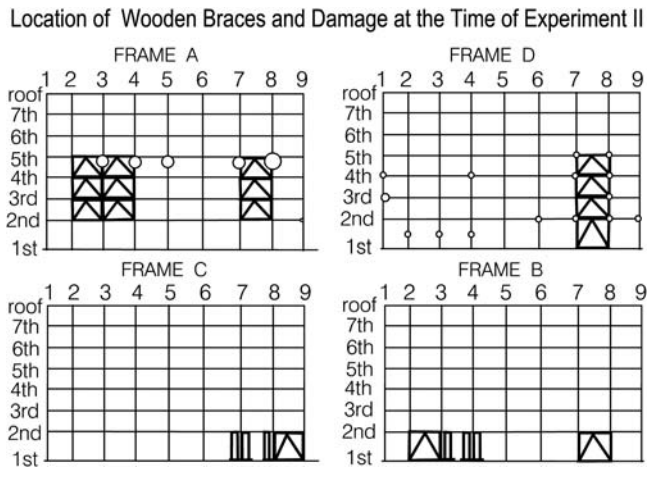

Figure 8. Schematic representation of the VN7SH structure, of its damage, and of wooden braces as seen at the time of experiment II (19 April 1994). Different sizes of open circles show schematically the degrees of damage in columns.

Figure 11 shows the rocking acceleration $\ddot{\theta}_y(t)$ in the VN7SH versus instantaneous system frequency f_p. It shows progressive reduction of f_p with increasing amplitude of response but again this reduction is not permanent. During ambient-vibration tests, f_p of the transverse (N–S) response is near 1.4 Hz and close to the value for the smallest earthquake motions (e.g., Montebello). Figure 11 also suggests that the soil–pile–foundation system during strong shaking behaves like a nonlinear system with gap elements (Fig. 10), which open during strong motion and can be closed by aftershock excitation.

Component Response

Migration of Centers of Torsion. The first torsional mode ($f = 1.6$ Hz) in VN7SH (Fig. 7) was seen in both the transverse and longitudinal microtremor vibrations, and both the longitudinal and transverse components of the modal displacement could be determined. Figure 12 shows the modal displacements in the plane of each floor. Figure 12a and b shows the results from experiments I (4–5 February 1994, before the wooden braces were added to strengthen the dam-

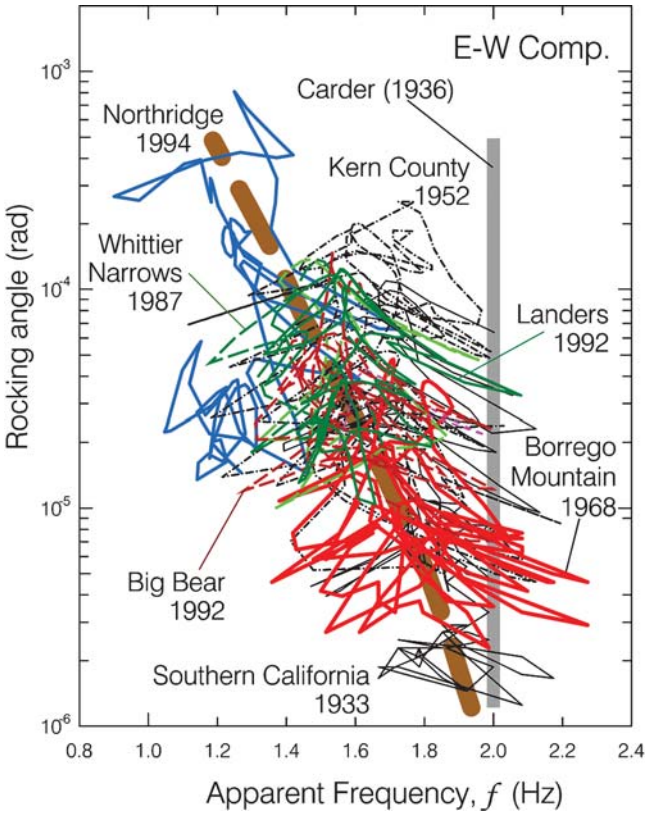

Figure 9. Dependence of apparent system frequency on amplitude of response (rocking angle) for E–W translation of HSB. Small-amplitude, ambient-vibration and forced-vibration estimates of system frequency by Carder (1936) are shown by the vertical gray line.

aged building) and II (19–20 April 1994, after the wooden braces were added, Fig. 8). The measurements were taken along longitudinal frame C. The most severely damaged columns were 3, 4, 5, 7, and 8 of longitudinal frame A (south of frame C) on the fifth floor.

The reinforced-concrete floor slabs of VN7SH are 8.5 inch thick, are stiff in their own plane, and translate and rotate about vertical axes. While the transverse component of motion is dominant, the response in the longitudinal direction is not small, especially for the top floors. During experiment I (Fig. 12a) the transverse component of motion changes phase but the longitudinal component does not. Also, the amplitudes of the longitudinal displacements are not proportional to the transverse displacements, as would be expected for a clean rotation. The longitudinal response of the middle columns (columns C4, C5, and C6) is seen at each floor, which indicates coupling of the torsion for this mode with the longitudinal response. The phase of the longitudinal response of the upper floors (roof, seventh, and sixth) is opposite from the one at the lower floors (third and fourth). The shaded oval zones in Figure 12a show the centers of rotation for the floor slabs, determined by drawing a normal to the displacement vectors. Because of measurement errors and some deformation of the floor slabs, the center of rotation for a floor slab is not a point but a zone. The centers of rotation are located south of frame C above the fifth floor, and north of frame C at the lower floors. At the lower floors, the centers are close to the middle (column 5) and then jump to the east part of the frame at the sixth floor. Between the sixth floor and the roof, they move toward the center of the frame. The jump from south to north is between the fifth and sixth floors, where the most severe damage occurred (Figs. 7 and 8). The results of experiment II (Fig. 12b) show that the centers of rotation are all south of frame C and are all near the center of the frame (near column line 5). This is explained by the action of added braces, which reduced torsional eccentricities due to the damaged columns at the fifth floor and mainly along (south) frame A (Figs. 7 and 8). This example shows that mapping discontinuities in the rotational response of full-scale structures can be a useful tool for locating damage in structural members.

Nonlinear Waves

Detection of damage in structures is one of the contemporary challenges in structural dynamics for powerful

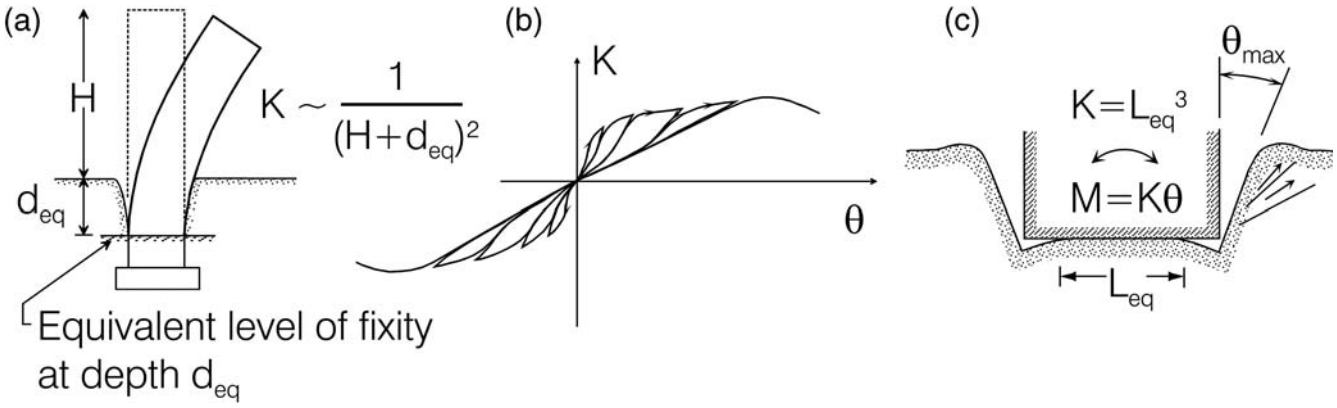

Figure 10. (a) Nonlinear changes in rocking stiffness caused by passive soil pressure on the sidewalls of the building and variable equivalent depth of fixity d_{eq}, (b) equivalent nonlinear system stiffness, and (c) schematic representation of permanent soil deformation after large rocking response.

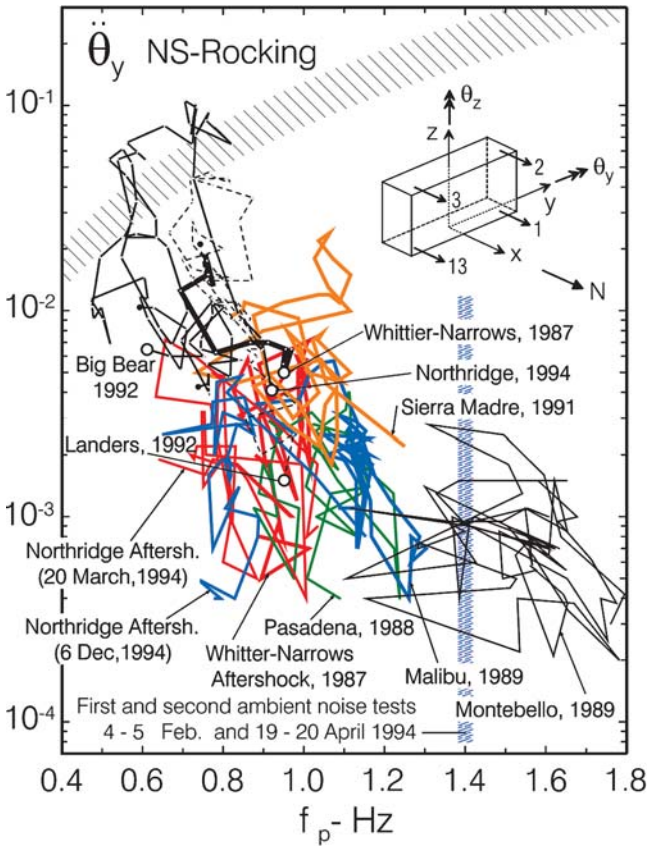

Figure 11. Peak amplitudes of $\ddot{\theta}_y$ (N–S rocking acceleration) versus f_p (apparent frequency of the soil–foundation–structure system) during 12 earthquakes recorded in the VN7SH building. The wide vertical line shows the apparent N–S frequency of the system response as determined from experiments I and II. The hatched zone near the top left-hand corner describes the range of typical code values for allowed drift in concrete structures.

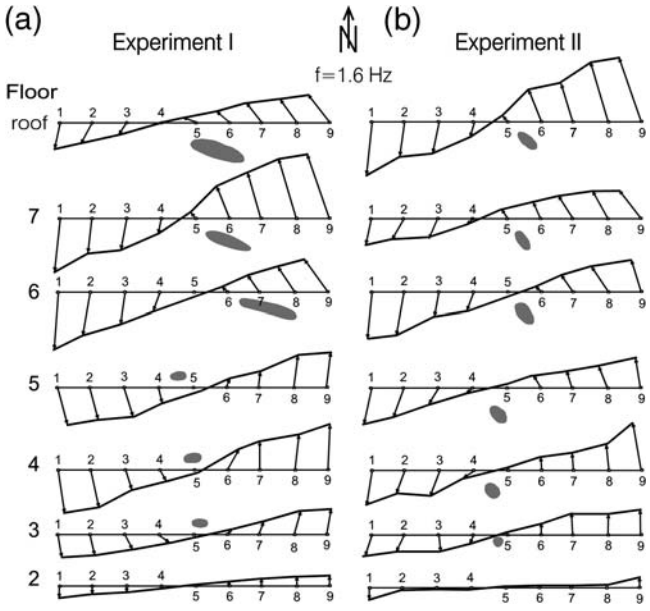

Figure 12. Displacements in the planes of the floor slabs at the frequency of the first torsional mode ($f = 1.6$ Hz). (a) Experiment I and (b) experiment II. The oval gray zones show centers of rotation. In (a), a jump in the position of the centers of rotation occurs between the fifth and sixth floors.

transient excitations by earthquakes, impact loads, and explosions. The goal of structural health monitoring is to detect the location, the extent, the nature, and the time of occurrence of the damage, in real time. Having detected the damage, the objective is then to provide a real-time means of dealing with its consequences. During propagation of damage (nonlinear waves) in structural members, point rotations will become large in the areas of strain localization. In the future, strategically placed rotational sensors will be used to detect initiation of damaging deformations, and the recorded data will be used to determine the location and the extent of damage. At present, in the absence of recorded data in full-scale structures, computer models are used to explore the nature of these large point rotations and to develop the detection algorithms (Gičev and Trifunac, 2008).

Discussion and Conclusions

Rotational components of strong ground motion are not currently considered in earthquake-resistant design. The sudden, large initial velocities in the ground motion near faults are also ignored. This is in part due to the lack of strong-motion records near the faults and to the absence, in free field and in structures, of instruments capable of recording rotational components of motion. The examples of fault motions described in this article include large initial velocities and are accompanied by sudden large rotations. Both have been shown to have profound effects on the response of structures near faults (Jalali and Trifunac, 2008) and to dominate in both linear and nonlinear responses. When combined with the effects of differential excitation of columns in the first story of extended structures, the complexity of the response, even for the simplest structures, becomes considerable—and very different from what is expected based on typical engineering analyses. It follows that ignoring the contribution of the rotational components of strong motion will result in underestimated drifts (Trifunac, 2009b). Therefore, for the development of sound engineering design, it is important to quantify the amplification of response caused by the rotational components of strong motion and to develop an understanding of how these additional excitations contribute to the response.

The eccentric location of foundations relative to the center of the mass of the structures makes the foundations the sources of rotational motions in the soil. Through the soil–structure interaction, the energy of the incident seismic waves is converted into the foundation rocking and torsion (Trifunac, 2008). For multiple foundations of long structures such as bridges, all of the aforementioned will hold for individual foundations, but additional rotational motions in the soil will result from differential motions of the supports and

from the wave-passage effects. These additional rotations will tend to be associated with longer wavelengths, comparable to the interfoundation distances of the multiple foundation systems, and thus they can be viewed as resulting from a couple, or from a chain of couples, whose component forces lie in the vertical plane (for in-plane excitation) or the horizontal plane (for out-of-plane excitation). In an urban setting, a distribution of buildings will act as an extended surface source area consisting of a large number of closely spaced sources of translational and rotational motions, which will cause the warping of the half-space surface in the near field and a seemingly random distribution of strong, high-frequency surface waves in the far field. For a distribution of buildings 1–50 stories high, the waves generated by the movement of their foundations will be in the range 0.1–10 Hz.

The aforementioned trends can be interpreted in terms of rigid foundations supporting a single-degree-of-freedom oscillator as a model of a simple building. Mutatis mutandis, many of the previously described phenomena can be generalized to interpret the rotational components in the free-field wave motions resulting from a broad spectrum of other eccentrically supported oscillators ranging, for example, from individual trees to large and small geological formations like those in Monument Valley in Utah, down to Meteora in Greece or Sigiria in Sri Lanka.

It is hoped that this review will contribute toward recognition that the rotational components that accompany the translations in earthquake motions are important, that they should be recorded during future earthquakes, and that they must be included in engineering analyses of structural response.

Data and Resources

No data were used in this article. Parts of some of the plots used in this article came from published sources listed in the references.

References

Agamennone, G. (1906). *La Registrazione dei Terremoti*, Casa Editrice "L'Ellettricista."

Ariman, T., and G. E. Muleski (1981). A review of the response of buried pipelines under seismic excitation, *Earthq. Eng. Struct. Dyn.* **9,** 133–151.

Baratta, M. (1895). Richerche storiche sugli apparechi sismici, *Ann. Uff. Cent. Met. Geodin. Ital.* **2,** no. 17,1, 3–37.

Biot, M. A. (1965). *Mechanics of Incremental Deformations*, Wiley, New York.

Bouchon, M., and K. Aki (1982). Strain and rotation associated with strong ground motion in the vicinity of earthquake faults, *Bull. Seismol. Soc. Am.* **72,** no. 5, 1717–1738.

Bycroft, G. N. (1980). Soil-foundation interaction and differential ground motions, *Earthq. Eng. Struct. Dyn.* **8,** 397–404.

Carder, D. S. (1936). Vibration observation, in *Earthquake Investigation in California 1934–1935*, Special Publication No. 201, U.S. Dept. of Commerce, Coast and Geodetic Survey, 49–106.

Cecchi, P. F. (1876). Sismografo elettrico a carte affumicate scorrevoli, *Atti dell' Acad. Pontif. dei Nouvi Lincei*, **29,** 421–428.

Chen, K.-C., B.-S. Huang, J.-H. Wang, W.-G. Huang, T.-M. Chang, R.-D. Hwang, H.-C. Chiu, and C.-C. Tsai (2001). An observation of rupture pulses of the 20 September 1999 Chi-Chi, Taiwan, earthquake from near-field seismograms, *Bull. Seismol. Soc. Am.* **91,** no. 5, 1247–1254.

Davison, C. (1927). *Founders of Seismology.* Cambridge U Press: Cambridge.

Denza, P. F. (1887). Osservazioni fatte all'Osservatoria di Moncalieri sul terremoto del 23 Febbrario 1887, *Bolletino Mensuale dell' Osservatorio Centrale Moncalieri* **2,** no. 7, 68–70.

Duke, C. M., J. E. Luco, A. R. Carriveau, P. J. Hradilek, R. Lastrico, and D. Ostrom (1970). Strong earthquake motion and site conditions: Hollywood, *Bull. Seismol. Soc. Am.* **60,** no. 4, 1271–1289.

Duvall, W. I., and D. E. Fogelson (1962). Review of criteria for estimating damage to residences from blasting vibrations, U.S. Dept. of the Interior, Bureau of Mines, Report of Investigations 5968.

Favaro, A. (1884). Contribuzioni alla storia della microsismologia, *Atti Ist. veneto Sci.*, **6,** no. 2, 91–103.

Ferrari, G. (2006). Note on the historical rotation seismographs, in *Earthquake Source Asymmetry, Structural Media and Rotation Effects*, R. Teisseyre, M. Takeo, and E. Majewski (Editors), Springer, Heidelberg, 367–376.

Fletcher, J., J. Boatwright, L. Haar, T. Hanks, and A. McGarr (1984). Source parameters for aftershocks of the Oroville, California, earthquake, *Bull. Seismol. Soc. Am.* **74,** no. 4, 1101–1123.

Foutch, D. A., J. E. Luco, M. D. Trifunac, and F. E. Udwadia (1975). Full-scale three-dimensional tests of structural deformations during forced excitation of a nine-story reinforced concrete building, in *Proc. of the U.S. National Conf. on Earthquake Engineering*, Ann Arbor, Michigan, 206–215.

Galitzin, B. (1902). Uber seimometrische beobahtungen, *Izv. Postyann. Tsent. Seism. Komm.* **1,** 1, 101–183.

Galitzin, B. (1904). Zur methodik der seismometrischen beobachtungen, *Izv. Postoyann. Tsent. Seism. Komm.* **1,** 3, 1–112.

Ghobarah, A. (2004). On drift limits associated with different damage levels, *Proc. of the International Workshop on Performance-Based Seismic Design*, Bled, Slovenia, 321–332.

Gičev, V, and M. D. Trifunac (2008). Rotations in a shear-beam model of a seven-story building caused by nonlinear waves during earthquake excitation, *Struct. Control Health Monit.* doi 10.1002/stc.264.

Graizer, V. M. (1980). On the determination of displacement from strong-motion accelerograms, in *Proc. of the 7th World Conf. on Earthquake Engineering*, Istanbul, 2**,** 391–394.

Graizer, V. M. (1989). Ob izmerenii naklona zemnoi poverhnosti vblizi epicentra vzriva, *Dokl. Akad. Nauk. S.S.S.R.., Geofiz.*, **305,** no. 2, 314–318.

Graizer, V. M. (2006). Tilts in strong ground motion, *Bull. Seismol. Soc. Am.* **96,** no. 6, 2090–2102.

Gutenberg, B. (1927). *Grundlagen der Erdbebenkunde*, University of Frankfurt a/M, 189 pp.

Hart, G. C., M. DiJulio, and M. Lew (1975). Torsional response of high-rise buildings, *J. Struct. Div. ASCE* **101,** 397–414.

Housner, G. W., and M. D. Trifunac (1967). Analysis of accelerograms—Parkfield earthquake, *Bull. Seismol. Soc. Am.* **57,** no. 6, 1193–1220.

Imamura, A. (1937). *Theoretical and Applied Seismology*, Maruzen Co., Tokyo, 358 pp.

Ivanović, S., M. D. Trifunac, E. I. Novikova, A. A. Gladkov, and M. I. Todorovska (1999). Instrumental 7-story reinforced concrete building in Van Nuys, California: ambient vibration survey following the damage from the 1994 Northridge earthquake, Dept. of Civil Engineering, University of Southern California, Los Angeles, California, Report Number CE 99–03, available at http://www.usc.edu/dept/civil_eng/Earthquake_eng/ (last accessed May 2008).

Jalali, R., and M. D. Trifunac (2008). A note on strength reduction factors for design of structures near earthquake faults, *Soil Dyn. Earthq. Eng.* **28,** no. 3, 212–222.

Kozák, J. T. (2006). Development of earthquake rotational effect study, in *Earthquake Source Asymmetry, Structural Media and Rotation Effects*, R. Teisseyre, M. Takeo, and E. Majewski (Editors), Springer, Heidelberg, 3–10.

Lee, V. W. (1979). Investigation of three-dimensional soil-structure interaction, Dept. of Civil Engineering, Univ. Southern California, Los Angeles, California, Report Number CE 79–11, available at http://www.usc.edu/dept/civil_eng/Earthquake_eng/ (last accessed May 2008).

Lee, V. W., and M. D. Trifunac (1985). Torsional accelerograms, *Soil Dyn. Earthq. Eng.* **4,** no. 3, 132–139.

Lee, V. W., and M. D. Trifunac (1987). Rocking strong earthquake accelerations, *Soil Dyn. Earthq. Eng.* **6,** no. 2, 75–89.

Lin, C. H., V. W. Lee, and M. D. Trifunac (2005). The reflection of plane waves in a poroelastic half-space saturated with inviscid fluid, *Soil Dyn. Earthq. Eng.* **25,** no. 3, 205–223.

Luco, J. E. (1976). Torsional response of structures to obliquely incident seismic *SH* waves, *Earthq. Eng. Struct. Dyn.* **4,** 207–219.

Luco, J. E., M. D. Trifunac, and F. E. Udwadia (1975). An experimental study of ground deformations caused by soil-structure interaction, in *Proc. of the U.S. National Conf. on Earthquake Engineering*, Ann Arbor, Michigan, 136–145.

Milne, J. (1893). A note on the great earthquake of October 28, 1891, *Seism. J. Japan* **1,** 127–151.

Richter, C. F. (1958). *Elementary Seismology*, Freeman and Co., San Francisco.

Sánchez-Sesma, F. J., V. J. Palencia, and F. Luzon (2002). Estimation of local site effects during earthquakes: An overview, *Indian Soc. Earthq. Technol. J.* **39,** no. 3, 167–194.

Schlüter, W. (1903). Schwingungsart und Weg der Erdbebenwellen, *Beitr. Geophys.* **5,** 314–359.

Teisseyre, R. (2002). Continuum with defect and self rotation fields, *Acta Geophys. Pol.* **50,** 51–68.

Teisseyre, R., and E. Majewski (2002). Physics of earthquakes, in *International Handbook of Earthquake and Engineering Seismology, Part A*, W. Lee, P. Jennings, C. Kisslinger, and H. Kanamori (Editors), Academic Press, New York, 229–235.

Teisseyre, R., J. Suchcicki, K. Teisseyre, J. Wiszniowski, and P. Palangio (2003). Seismic rotation waves: Basic elements of theory and recording, *Ann. Geophys.* **46,** no. 4, 671–685.

Todorovska, M. I. (2002). Full-scale experimental studies of soil-structure interaction, *Indian Soc. Earthq. Technol. J.* **39,** no. 3, 139–166.

Todorovska, M. I. (2009). Soil-structure system identification of Milikan Library north–south response during four earthquakes (1970–2002): what caused the observed wandering of the system frequencies?, *Bull. Seismol. Soc. Am.* **99,** 626–635.

Todorovska, M. I., and M. D. Trifunac (2008). Impulse response analysis of the Van Nuys 7-story hotel during 11 earthquakes and earthquake damage detection, *Struct. Control Health Monit.* **15,** no. 1, 90–116.

Trifunac, M. D. (1972a). Stress estimates for San Fernando, California, earthquake of February 9, 1971: Main event and thirteen aftershocks, *Bull. Seismol. Soc. Am.* **62,** no. 3, 721–750.

Trifunac, M. D. (1972b). Tectonic stress and source mechanism of the Imperial Valley, California, earthquake of 1940, *Bull. Seismol. Soc. Amr.* **62,** no. 5, 1283–1302.

Trifunac, M. D. (1972c). Interaction of a shear wall with the soil for incident plane *SH* waves, *Bull. Seismol. Soc. Am.* **62,** no. 1, 63–83.

Trifunac, M. D. (1976). Preliminary analysis of the peaks of strong earthquake ground motion-dependence of peaks on earthquake magnitude, epicentral distance and the recording site conditions, *Bull. Seismol. Soc. Am.* **66,** no. 1, 189–219.

Trifunac, M. D. (1982). A note on rotational components of earthquake motions for incident body waves, *Soil Dyn, Earthq. Eng.* **1,** no. 1, 11–19.

Trifunac, M. D. (1993). Broad-band extension of Fourier amplitude spectra of strong motion acceleration, Dept. of Civil Engineering, University of Southern California, Los Angeles, California, Report Number CE 93–01, available at http://www.usc.edu/dept/civil_eng/Earthquake_eng/ (last accessed May 2008).

Trifunac, M. D. (1998). Stresses and intermediate frequencies of strong motion acceleration, *Geofizika* **14,** 1–27.

Trifunac, M. D. (2006). Effects of torsional and rocking excitations on the response of structures, in *Earthquake Source Asymmetry, Structural Media and Rotation Effects*, R. Teisseyre, M. Takeo, and E. Majewski (Editors), Springer, Heidelberg, 569–582.

Trifunac, M. D. (2008). Buildings as sources of rotational waves, in *Physics of Asymmetric Continuum: Extreme and Fracture Processes*, R. Teisseyre, H. Nagahama, and E. Majewski (Editors), Springer, Heidelberg, Germany.

Trifunac, M. D. (2009a). 75th Anniversary of strong motion observation—A historical review *Soil Dyn. Earthq. Eng.* doi doi:10.1016/j.soildyn.2008.05.011.

Trifunac, M. D. (2009b). The role of strong motion rotations in the response of structures near earthquake faults, *Soil Dyn. Earthq. Eng.* **29,** no. 2, 382–393, doi 10.1016/j.soildyn.2008.04.001.

Trifunac, M. D., and V. Gičev (2006). Response spectra for differential motion of columns, paper II: Out-of-plane response, *Soil Dyn. Earthq. Eng.* **26,** no. 12, 1149–1160.

Trifunac, M. D., and D. E. Hudson (1971). Analysis of the Pacoima Dam accelerogram, San Fernando, California, earthquake of 1971, *Bull. Seismol. Soc. Am.* **61,** no. 5, 1393–1411.

Trifunac, M. D., and S. S. Ivanović (2003). Analysis of drifts in a seven-story reinforced concrete structure, Dept. of Civil Engineering, University of Southern California, Los Angeles, California, Report Number CE 03–01, available at http://www.usc.edu/dept/civil_eng/Earthquake_eng/ (last accessed May 2008).

Trifunac, M. D., and E. I. Novikova (1995). Duration of earthquake fault motion in California, *Earthq. Eng. Struct. Dyn.* **24,** no. 6, 781–799.

Trifunac, M. D., and M. I. Todorovska (1997a). Response spectra and differential motion of columns, *Earthq. Eng. Struct. Dyn.* **26,** no. 2, 251–268.

Trifunac, M. D., and M. I. Todorovska (1997b). Northridge, California, earthquake of 17 January 1994: density of pipe breaks and surface strains, *Soil Dyn. Earthq. Eng.* **16,** no. 3, 193–207.

Trifunac, M. D., and M. I. Todorovska (1998). Nonlinear soil response as a natural passive isolation mechanism—the 1994 Northridge, California, earthquake, *Soil Dyn. Earthq. Eng.* **17,** no. 1, 41–51.

Trifunac, M. D., and M. I. Todorovska (2001a). A note on usable dynamic range in accelerographs recording translation, *Soil Dyn. Earthq. Eng.* **21,** no. 4, 275–286.

Trifunac, M. D., and M. I. Todorovska (2001b). Recording and interpreting earthquake response of full-scale structures, *Proc. of the NATO Advanced Research Workshop on Strong-Motion Instrumentation for Civil Engineering Structures*, 2–5 June 1999, Istanbul, Turkey, Kluwer Academic Publishers, Dordrecht, 131–155.

Trifunac, M. D., T. Y. Hao, and M. I. Todorovska (2001). Response of a 14 story reinforced concrete structure to excitation by nine earthquakes: 61 years of observation in the Hollywood Storage Building, Dept. of Civil Engineering, University of Southern California, Los Angeles, California, Report Number CE 01–02, available at http://www.usc.edu/dept/civil_eng/Earthquake_eng/ (last accessed May 2008).

Trifunac, M. D., S. S. Ivanović, M. I. Todorovska, E. I. Novikova, and A. P. Gladkov (1999). Experimental evidence for flexibility of a building foundation supported by concrete friction piles, *Soil Dyn. Earthq. Eng.* **18,** no. 3, 169–187.

Trifunac, M. D., S. S. Ivanović, and M. I. Todorovska (1999). Seven story reinforced concrete building in Van Nuys, California: Strong motion data recorded between 7 February 1971 and 9 December 1994, and description of damage following Northridge, 17 January 1994 earthquake, Dept. of Civil Engineering, University of Southern California, Los Angeles, California, Report Number 99–02, available at

http://www.usc.edu/dept/civil_eng/Earthquake_eng/ (last accessed May 2008).

Trifunac, M. D., M. I. Todorovska, and S. S. Ivanovic (1996). Peak velocities, and peak surface strains during Northridge, California, earthquake of 17 January 1994, *Soil Dyn. Earthq. Eng.*, **15,** no. 5, 301–310.

Trifunac, M. D., M. I. Todorovska, and V. W. Lee (1998). The Rinaldi strong motion accelerogram of the Northridge, California, earthquake of 17 January 1994, *Earthq. Spectra* **14,** no. 1, 225–239.

Werner, S. D., L. C. Lee, H. L. Wong, and M. D. Trifunac (1979). Structural response to traveling seismic waves, *J. Struct. Div. ASCE* **105,** no. ST12, 2547–2564, available at http://www.usc.edu/dept/civil_eng/Earthquake_eng/ (last accessed May 2008).

Wiechert, E. (1903). Theorie der automatischen Seismographen, *Abh. K. Bes. Wiss. Göttingen* Klasse N. F. **2,** no. 1902–1903, 1–128.

Wong, H. L., and M. D. Trifunac (1975). Two-dimensional, antiplane, building-soil-building interaction for two or more buildings and for incident plane *SH* waves, *Bull. Seismol. Soc. Am.* **65,** 1863–1885.

Wong, H. L., J. E. Luco, and M. D. Trifunac (1977). Contact stresses and ground motion generated by soil-structure interaction, *Earthq. Eng. Struct. Dyn.* **5,** no. 1, 67–79.

Department of Civil Engineering
University of Southern California
Los Angeles, California 90089

Manuscript received 15 May 2008